Chemistry and Physics of Lipids 234 (2021) 105018

Contents lists available at ScienceDirect

Chemistry and Physics of Lipids

journal homepage: www.elsevier.com/locate/chemphyslip

The interaction of a thiosemicarbazone derived from *R* - (+) - limonene with lipid membranes

C.A. Marquezin [a,*], C.M.A. de Oliveira [b], F. Vandresen [c], E.L. Duarte [d], M.T. Lamy [d], C.C. Vequi-Suplicy [e]

[a] *Instituto de Física, Universidade Federal de Goiás, CEP 74690-900, Goiânia, GO, Brazil*
[b] *Instituto de Química, Universidade Federal de Goiás, CEP 74690-900, Goiânia, GO, Brazil*
[c] *Federal Technological University of Paraná, CEP 86036370, Londrina, PR, Brazil*
[d] *Instituto de Física, Universidade de São Paulo, Rua do Matão 1371, CEP 05508-090, São Paulo, SP, Brazil*
[e] *IMDEA Nanociencia, Campus Universitario de Cantoblanco, 28049, Madrid, Spain*

ARTICLE INFO

Keywords:
Thiosemicarbazones
Limonene
Laurdan
DMPC
Fluorescence
ESR
DSC

ABSTRACT

As a potential drug, *2-nitrobenzaldehyde-thiosemicarbazone* (2-TSC), a thiosemicarbazone derived from the terpene R-(+)-limonene, was studied through calorimetric and spectroscopic techniques. Differential Scanning Calorimetry (DSC) data showed that 2-TSC causes structural changes in a *1,2-dipalmitoyl*-sn-*glycero-3-phosphocholine* (DMPC) membrane, strongly decreasing the cooperativity of the bilayer gel-fluid thermal transition. Optical absorption spectroscopy showed that 2-TSC is more soluble in ethanol and lipids than in water medium, and that the drug displays different structures in the different environments. Though 2-TSC displays no fluorescence, time resolved fluorescence showed that the drug is an effective quencher of the fluorescent probe *6-dodecanoyl-2-dimethylaminonaphthalene* (Laurdan). As it is well accepted that Laurdan is positioned into the bilayer close to the membrane surface, that is possibly the localization of 2-TSC in a bilayer. Electron spin resonance (ESR) of the probe *1-palmitoyl-2-stearoyl-(14-doxyl)-sn-glycero-3-phosphocholine* (14-PCSL) revealed that 2-TSC is inserted into the hydrocarbon part of the bilayer, fluidizing the lipid bilayer gel phase and rigidifying or organizing the bilayer fluid phase. Similar effects are found for other lipophilic molecules, including cholesterol. These results are useful to improve the understanding of the processes that govern the interaction of thiosemicarbazones with cell membranes, related to the activity of the drugs and their cytotoxicity.

1. Introduction

Thiosemicarbazones (TSC) are an important class of compounds developed for organic and analytical chemistry, which exhibit a wide range of biological activities. They have been recognized for their antibacterial, antiviral, antifungal and antiparasitic properties (De Farias Santiago et al., 2014; Glinma et al., 2014; Magalhaes Moreira et al., 2014; Mohamed et al., 2014; Soares et al., 2011; Yu et al., 2009). They still exhibit antineoplastic potential against leukemia cells (da Silva et al., 2010; Shyamsivappan et al., 2020; Vandresen et al., 2014) and human colon cancer cell line (Ali et al., 2014). Recently, Sundus N. Maqbool et al. 2019 showed that TSC combined with tamoxifen presented high potential as an alternative therapy for the treatment of breast cancer (Maqbool et al., 2020).

All these properties prompted many authors to synthesize these molecules connected with different chemical groups, like a thiophene (de Araújo Neto et al., 2020), a thiazolidine (Trotsko et al., 2020), a quinoline (Shyamsivappan et al., 2020) or an indol (da Silva et al., 2020). Other authors have complexed TSC and some derivatives with inorganic elements, like cobalt (Beebe et al., 2020), ruthenium (Yildirim et al., 2014), manganese-iron (Lawrence et al., 2020) and gold (González-Barcia et al., 2020).

It is also possible to obtain a TSC molecule from a terpene unit. These thiosemicarbazones derived from terpenes have been synthesized in Brazil (da Silva et al., 2010; Haraguchi et al., 2011), due to terpenes being abundantly found in the Brazilian flora (Yamaguchi et al., 2009). Terpenes are commonly present in volatile oils, with a basic structure of isopropene (C_5H_8), and have been shown to be active against a variety of tumors (Haag et al., 1992; Maqbool et al., 2020; Jaroque et al., 2020) and pathogenic parasites (Alonso et al., 2019; Camargos et al., 2014;

* Corresponding author.
E-mail address: cassia_m@ufg.br (C.A. Marquezin).

https://doi.org/10.1016/j.chemphyslip.2020.105018
Received 5 September 2020; Received in revised form 14 November 2020; Accepted 16 November 2020
Available online 21 November 2020

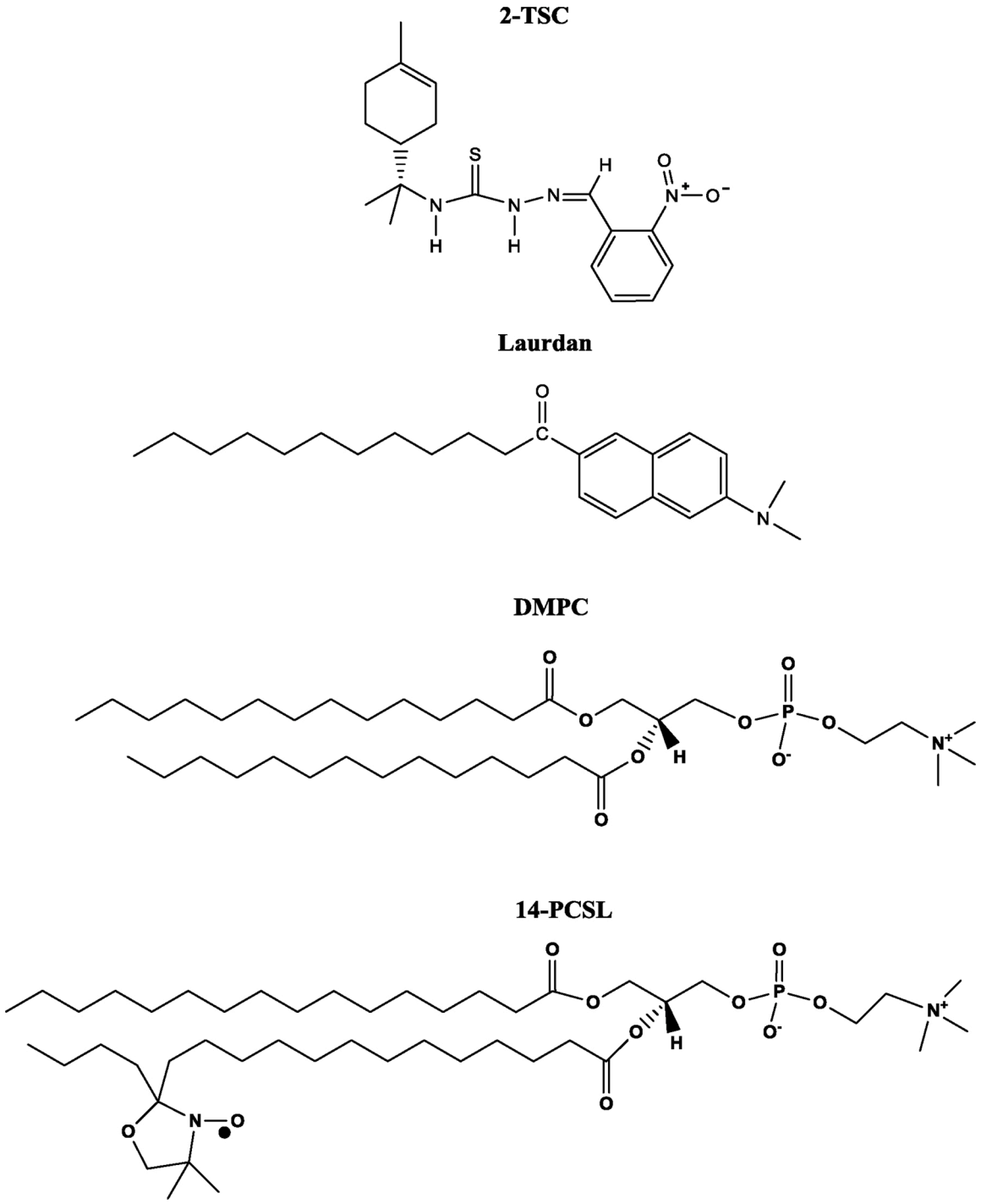

Fig. 1. Chemical structures of the compounds used in this work, as indicated.

Menezes et al., 2014), such as *Leishmania* and *Trypanosoma cruzi*. For example, the 4-methyl-1-isoprenyl cyclohexene (limonene), a monocyclic monoterpene, is part of the structure of more than 300 plants (Asamoto et al., 2002), and displays antifungal and antibacterial activities (Mourey and Canillac, 2002; Ozturk and Ercisli, 2006; Singh et al., 2010). There are some thiosemicarbazones derived specifically from limonene, that have shown antiproliferative properties in tumor cells (Vandresen et al., 2014) and caused cell death and ultra-structural alterations in *Leishmania amazonensis* (Britta et al., 2014). Terpenes also behave as strong enhancers of the permeability of the skin (Chen et al., 2016; dos Anjos and Alonso, 2008; Hatta et al., 2010; Lim et al., 2006), and due to their lipid membrane affinity, terpenes were found to contribute to the increase of the fluidity of lipid bilayers (Alonso et al., 2016; Mendanha et al., 2017; Mendanha and Alonso, 2015).

Most of the works found in the literature on thiosemicarbazones are related to their biological activity, and few are the studies about their physicochemical and spectroscopic properties, or studies that monitor their interactions with cell membranes at the molecular level, through biophysical methods. Often the cytotoxicity of a drug lies in the fact that this drug is hydrophobic and has the ability to cause significant changes in a cell membrane. Then, in order to better understand the mechanisms of action and the behavior of these molecules in the presence of lipid bilayers, we present in this work an optical spectroscopic study of a new thiosemicarbazone derived from R-limonene, *the 2-nitrobenzaldehyde-*

thiosemicarbazone (Vandresen et al., 2014) (in this work, called 2-TSC), both in water medium and in lipid membranes. Moreover, with Differential Scanning Calorimetry (DSC), we show that 2-TSC is inserted into the lipid bilayer, as it can change the thermal behavior of a *1,2-dimyristoyl-sn-glycero-3-phosphocholine* (DMPC) membrane.

Fluorescence and electron spin resonance (ESR) spectroscopies also showed the interaction between 2-TSC and DMPC vesicles, and they evinced the structural changes caused in the lipid bilayer due to the presence of this molecule. The fluorescent probe used was *6-dodecanoyl-2-dimethylaminonaphthalene* (Laurdan) (Calori et al., 2019; Chilom et al., 2020; Leung et al., 2019; Ma et al., 2018; Osella et al., 2019; Pérez et al., 2019; Vequi-Suplicy et al., 2013), and *1-palmitoyl-2-stearoyl-(14-doxyl)-sn-glycero-3-phosphocholine* (14-PCSL) (Dave et al., 2004) was used in ESR measurements.

2. Materials and methods

2-nitrobenzaldehyde-thiosemicarbazone (2-TSC) was prepared as previously described (Vandresen et al., 2014). *6-dodecanoyl-2-dimethylaminonaphthalene* (Laurdan) was purchased from Molecular Probes Inc. (Eugene, OR, USA). The phospholipid *1,2-dimyristoyl-sn-glycero-3-phosphocholine* (DMPC) and the spin label *1-palmitoyl-2-stearoyl-(14-doxyl)-sn-glycero-3-phosphocholine* (14-PCSL) were supplied by Avanti Polar Lipids Inc. (Birmingham, AL, USA). *4-(2-hydroxyethyl)-1-piperazineethanesulfonic acid* (HEPES), chloroform, NaOH and HCl were purchased from Sigma Aldrich (St Louis, MO). All compounds were used without further purification. Milli-Q water was used throughout. Fig. 1 shows the chemical structures of the main compounds used here.

2.1. Liposome preparation

Liposomes were prepared as previously described (Hope et al., 1985). Briefly, 1 mM lipid was dissolved in chloroform. The sample was dried with nitrogen and the solvent completely removed under reduced pressure to obtain the dried lipid film.

For absorption and fluorescence spectroscopy, the fluorophore Laurdan was added to the lipid/chloroform solution at 1 mol% of the lipid concentration. For electron spin resonance (ESR) measurements, the spin label 14-PCSL was added to the lipid/chloroform solution at 0.3 mol% of the lipid concentration. All experiments were performed in the absence and presence of four different 2-TSC concentrations (1, 5, 10 and 15 mol% of the lipid concentration, corresponding to 10, 50, 100 and 150 μM of 2-TSC, respectively). They were also mixed with the lipid/chloroform solution.

The lipid films were hydrated in buffer solution (HEPES 10 mM pH 7.4) to obtain a 1 mM lipid concentration and vortexed. The suspension was than extruded 21 times through polycarbonate membranes, using a Mini Extruder from Avanti Polar Lipids Inc. (Birmingham, AL, USA). The extrusion was made using 0.1 μm pore diameter polycarbonate membranes (from Millipore), resulting in a population of monodisperse Large Unilamellar Vesicles (LUV), with average diameter of 0.1 μm.

2.2. Differential scanning calorimetry (DSC)

DSC data were obtained with a Microcalorimeter (Microcal VP-DSC, Northampton, MA, USA). Temperature was varied from 5 up to 50 °C, at a scan rate of 20 °C/h. The lipid concentration was 1 mM for all samples. Baseline subtractions and peak integrals were done with the MicroCal Origin software provided by MicroCal, as described before (Riske et al., 2009). All DSC data were obtained in duplicate. Very similar scans were obtained from different preparations for each dispersion.

2.3. Optical absorption spectroscopy

Optical absorption spectra were obtained with an UV – Vis spectrophotometer (Varian Cary, Santa Clara, CA). Samples were placed in quartz cuvettes, with absorption optical pathway of 2 mm. The temperature was controlled with a Carry Peltier thermostat. To ensure thermal equilibrium, before each scan the sample was left at the desired temperature for at least 10 min.

2.4. Fluorescence spectroscopy

For steady state fluorescence spectroscopy, samples were placed in quartz cuvettes with 2 mm optical pathway. Measurements were performed using the Varian Cary Eclipse. The temperature was controlled by a Peltier system. To ensure thermal equilibrium, before each scan the sample was left at the desired temperature for at least 10 min. Emission spectra were measured with excitation wavelength at 330 nm for Laurdan, used here as a fluorescent membrane probe.

Steady state anisotropy data were obtained with the same equipment, using polarizers in the emission and excitation channels. The steady-state anisotropy, *r*, is given by:

$$r = \frac{I_{VV} - GI_{VH}}{I_{VV} + 2GI_{VH}} \quad (1)$$

where I_{VV} and I_{VH} are the intensities with the excitation polarizer at the vertical position, and the emission polarizer at vertical and horizontal positions, respectively, and G is the ratio of the sensitivity of the system for vertically and horizontally polarized light (Lakowicz, 2006). The excitation and emission wavelengths were, respectively, 330 nm and 480 nm.

2.5. Time-resolved fluorescence measurements

Time-resolved fluorescence measurements were performed using the time-correlated single photon counting method (TCSPC) (Lakowicz, 2006). The excitation source used was a titanium-sapphire laser Tsunami 3950 from Spectra Physics, pumped by a solid-state laser Millenia Pro model J80, also from Spectra Physics. The repetition rate was set to 8000 kHz using a pulse picker (Spectra Physics, model 3980−25). The Tsunami was set to give an output of 990 nm and a third harmonic generator BBO crystal (GWN-23PL Spectra Physics) was used to generate the excitation beam at 330 nm. This beam was directed to a spectrofluorometer from Edinburgh (FL900CDT). The emitted light was detected at 90° from the excitation beam. The emission wavelength was selected by a refrigerated microchannel plate photomultiplier (Hamamatsu R3809U). The FWHM of the instrument response function was 90–110 ps. Time resolution was 12 ps per channel. The temperature was controlled within 0.1 °C by the thermal bath Julabo HP 25. Excitation wavelength was at 330 nm, and the emission detected at 480 nm.

Software from Edinburgh Instruments was used to analyze the decay curves. The intensity decays were fitted to the equation (Lakowicz, 2006):

$$I(t) = \sum_i \alpha_i e^{-t/\tau_i} \quad (2)$$

where τ_i is the lifetime of the *i*th component of the decay, and α_i is the corresponding pre-exponential factor.

2.6. Electron spin resonance (ESR) spectroscopy

ESR measurements at X band (9.44 GHz) were performed with an EMX spectrometer (Bruker, Germany) using a high sensitivity ER4119HS cavity. The sample temperature was controlled within 0.1 °C by a Bruker BVT-2000 variable temperature device, and varied from 10 to 40 °C. To ensure thermal equilibrium, before each scan the sample was left at the desired temperature for at least 10 min. ESR data were acquired immediately after sample preparation. Field-modulation amplitude of 1 G and microwave power of 12 mW were used. The

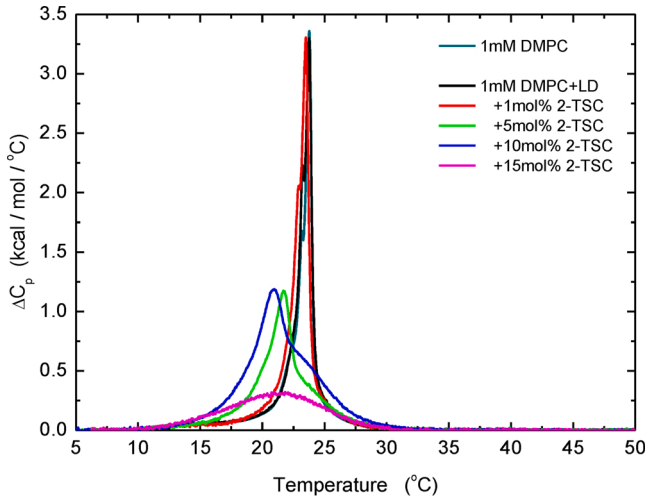

Fig. 2. Typical DSC thermograms of extruded DMPC (1 mM) and DMPC (1 mM) + Laurdan (1 mol%) in the absence and presence of different concentrations of 2-TSC. Scan rate was 20°C/h.

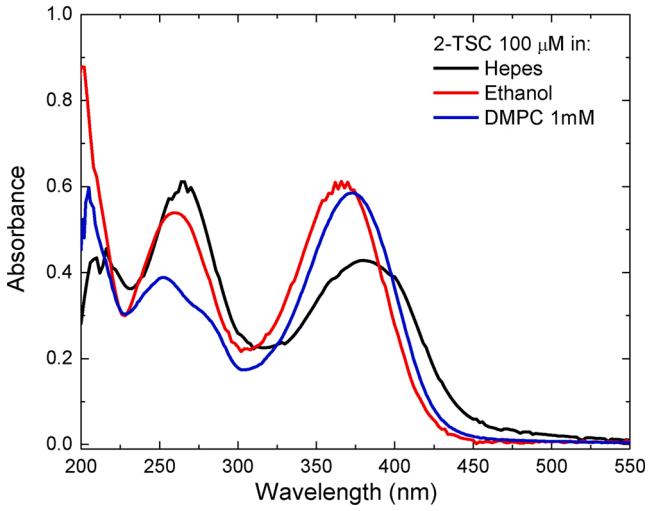

Fig. 3. Absorption spectra of 2-TSC (100 μM) in (—) HEPES buffer, (—) Ethanol and (—) DMPC (1 mM). All spectra were obtained at room temperature, 25°C.

Table 1
Parameters obtained from DSC thermograms (Fig. 2): main phase transition temperature (T_m), half maximum width of the transition peak ($\Delta T_m^{1/2}$) and the enthalpy variation (ΔH_m), for extruded 1 mM of pure DMPC and 1 mM DMPC + Laurdan 1 mol%, in the absence and presence of different concentrations of 2-TSC.

	T_m (°C)	$\Delta T_m^{1/2}$ (°C)	ΔH_m (kcal/mol)
[1 mM] DMPC	23.8 ± 0.1	0.7 ± 0.1	5.0 ± 0.3
[1 mM] DMPC + LD			
+ 0 mol% 2-TSC	23.8 ± 0.1	0.9 ± 0.1	5.2 ± 0.3
+ 1 mol% 2-TSC	23.3 ± 0.2	1.1 ± 0.1	5.5 ± 0.4
+ 5 mol% 2-TSC	21.6 ± 0.1	2.6 ± 0.3	4 ± 1
+ 10 mol% 2-TSC	20.9 ± 0.1	4.0 ± 0.3	5 ± 1
+ 15 mol% 2-TSC	21.3 ± 0.5	9.0 ± 0.2	2.5 ± 0.5

spin probe 14-PCSL was used.

All data shown here are means of at least two experiments, and the uncertainties are the standard deviations. When not shown, uncertainties were found to be smaller than the size of the symbols.

3. Results and discussion

In this work, 2-TSC was studied for the first time in the presence of a phospholipid membrane, as a model for a cell membrane. As observed for some drugs, one of the mechanisms of action against a pathogenic organism is through the interaction of the drug with its cell membrane.

3.1. DSC measurements

Saturated lipid bilayers often display a very narrow peak of heat capacity, which is characteristic of a cooperative process, being very dependent on lipid-lipid interaction. As the presence of an exogenous molecule may interfere with the phase transition process, DSC thermograms can provide important information about the interaction of exogenous molecules with lipid systems. In particular, 100 nm extruded lipid dispersions of DMPC (Large Unilamellar Vesicles, LUVs) exhibit a cooperative main transition peak around 23 °C (Katsaras and Gutberlet, 2001; Marsh, 1990). Calorimetric measurements were performed with 1 mM DMPC extruded vesicles in the absence and presence of 1, 5, 10 and 15 mol% of 2-TSC relative to the lipid concentration, corresponding to 10, 50, 100 and 150 μM of 2-TSC, respectively. The fluorescent probe Laurdan (at 1 mol%) was present in all samples with 2-TSC, once it was required for fluorescence spectroscopy studies. In order to check if Laurdan, at the used concentration, was able to modify the thermal profile of the lipid bilayer, a control sample of pure 1 mM DMPC extruded vesicles, without the fluorescent probe, was prepared. DSC heating scans are shown in Fig. 2, and important thermal parameters extracted from DSC scans are found in Table 1.

As expected, a typical thermal event was observed for the extruded DMPC dispersion, with a narrow peak at 23.8 °C and enthalpy variation, ΔH_m, around 5 kcal/mol (Katsaras and Gutberlet, 2001; Marsh, 1990), and no significative difference was observed in the absence or presence of the probe Laurdan (Fig. 2 and Table 1), indicating that the probe (at low concentration, 1 mol%) does not cause any alteration on the DMPC membrane. It is important to have in mind that extruded DMPC does not present the pre-transition (Enoki et al., 2012). With the addition of 2-TSC at 1 mol%, a very small decrease in the transition temperature can be seen without any effect on the half maximum width of the transition peak, $\Delta T_m^{1/2}$ or ΔH_m, comparing with DMPC without 2-TSC. The increase of 2-TSC causes a decrease of the main temperature and a strong broadening of the peak (Fig. 2 and Table 1), revealing that 2-TSC strongly reduces the gel-fluid transition cooperativity. Therefore, 2-TSC molecules interact with lipid membranes of DMPC, decreasing the lipid-lipid cooperativity. However, only the highest 2-TSC concentration used here, 15 mol%, caused a decrease on the gel-fluid transition enthalpy, ΔH_m (Table 1). That means that only at 15 mol% 2-TSC the total energy required for the melting of the hydrocarbon chains decreases significantly (Heimburg, 2007).

It is important to note that the DMPC and 2-TSC concentrations used to obtain the DSC thermograms are the same used in the optical absorption experiments described below, and no evidence of 2-TSC/2-TSC interaction was detected at these concentrations. (Figs. 4c and Fig. 5).

3.2. Absorption spectroscopy

For the spectroscopic characterization of 2-TSC, Fig. 3 shows the optical absorption spectra of 2-TSC in HEPES buffer, ethanol and DMPC vesicles. The absorption spectrum shows at least two bands in aqueous solution and in ethanol. In the presence of DMPC, there is a clear split of the higher energy band (lower wavelength) into at least two other bands, with peaks around 253 and 276 nm.

In DMPC, the lower energy band (peak at 373 nm) is located closer to the ethanol band (peak at 367 nm) than the HEPES band (380 nm). The 2-TSC band in DMPC is as narrow as that in ethanol. Considering the dielectric constant of the aqueous medium as 80 and that of ethanol as

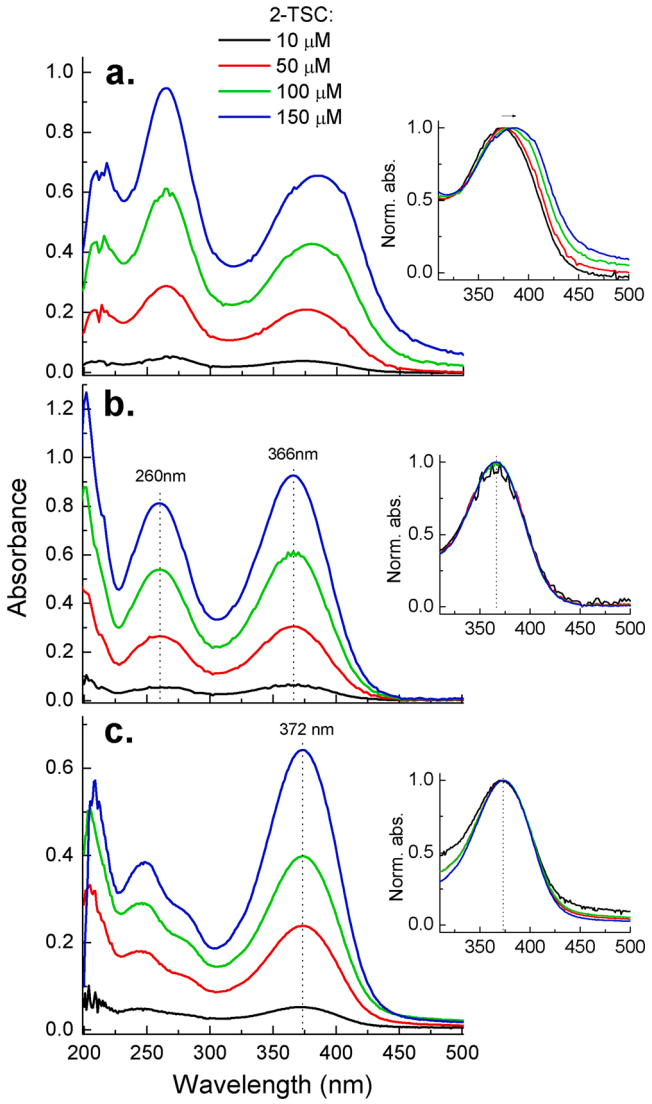

Fig. 4. Absorption spectra of 2-TSC as a function of its concentration in HEPES Buffer (a), ethanol (b) and 1 mM DMPC (c). All spectra were obtained at room temperature, 25°C. When shown, dotted lines indicate no shift in the main bands with the increasing concentration of 2-TSC. The insets correspond to the normalized low energy bands.

24.5, we could infer that 2-TSC molecule is positioned in the lipid bilayer, in a region of dielectric constant value between 24.5 and 80. Clearly, this region is not in the deep part of the fatty acid chains, where the dielectric constant would be much lower, neither at the bilayer surface: 2-TSC appears to be partially inserted in the region of the polar head groups or just below them, where some water molecules are still present.

Optical spectra in HEPES buffer, ethanol and DMPC vesicles were also obtained for different concentrations of 2-TSC, as shown in Fig. 4. In ethanol and DMPC, there is no significant spectral shift for all bands, with the increasing of 2-TSC concentration (see insets in Fig. 4 for the normalized low energy absorption band). However, in HEPES buffer (Fig. 4a) the lower energy band shifts to longer wavelengths as the 2-TSC concentration increases. Moreover, there seems to be an increase in the sample light scattering, as indicated by the increase in the Absorbance at 500 nm (Fig. 4a, and Fig. S1 in SM). The change in the 2-TSC optical spectrum as the molecule concentration increases, and the appearance of light scattering, are strongly indications of molecular aggregation in HEPES buffer.

The values of the maximum Absorbance at the low energy bands are

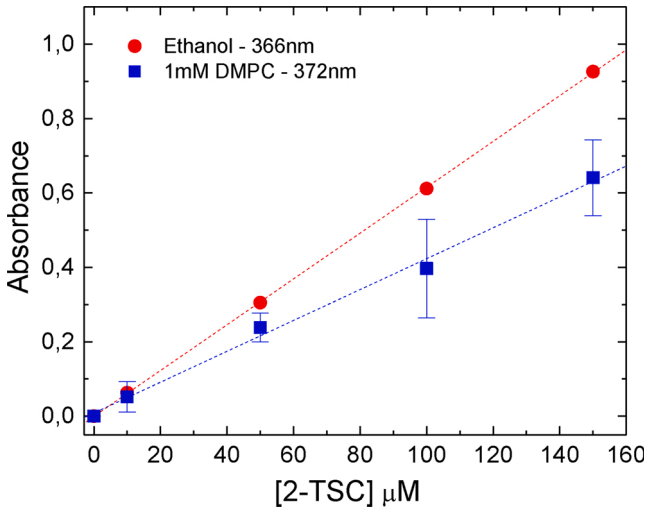

Fig. 5. Absorbance values for different concentrations of 2-TSC in Ethanol at 366 nm and in DMPC at 372 nm. All measurements were made at room temperature. Dashed lines are the best linear fittings of the experimental data.

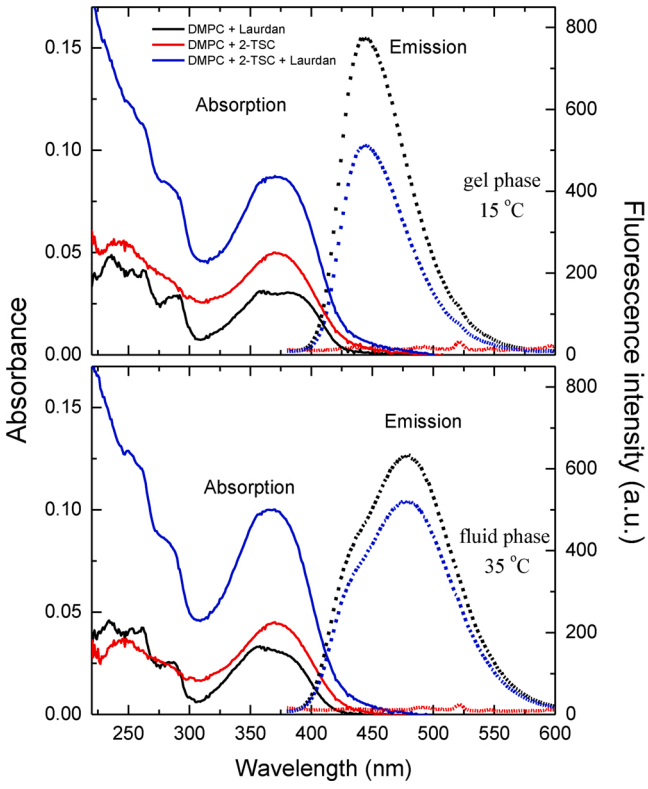

Fig. 6. Optical absorption (solid lines) and emission spectra (dot lines) of 2-TSC (1 mol%) and Laurdan (1 mol%), in the presence of DMPC vesicles (1 mM), in gel phase (15 °C) and in fluid phase (35 °C). Excitation wavelength was 330 nm.

plotted *versus* the concentration of the compound, Fig. 5, for 2-TSC in ethanol and DMPC. Through the use of the Lambert-Beer law (Valeur, 2001), we calculated the molar absorption coefficient (ε) of 2-TSC for each medium: $\varepsilon_{ethanol} = (31 \pm 4)10^3\ cm^{-1}M^{-1}$ and $\varepsilon_{DMPC} = (29 \pm 8)10^3\ cm^{-1}M^{-1}$, at 366 nm and 372 nm, respectively. These high values of molar absorption coefficient, together with the red shift observed when switching from ethanol to HEPES buffer suggest that the lower energy band is associated with a $\pi \rightarrow \pi^*$ transition.

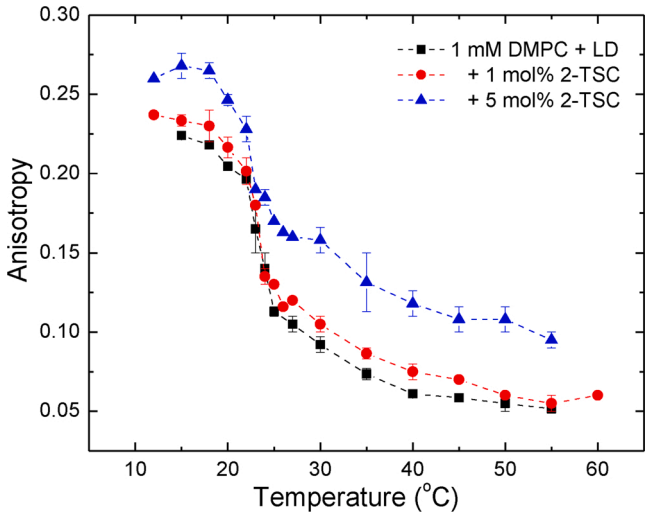

Fig. 7. Values of steady state anisotropy of Laurdan (1 mol%) in DMPC vesicles, with 1 mol% and 5 mol % of 2-TSC. Excitation wavelength at 330 nm, and emission wavelength at 480 nm.

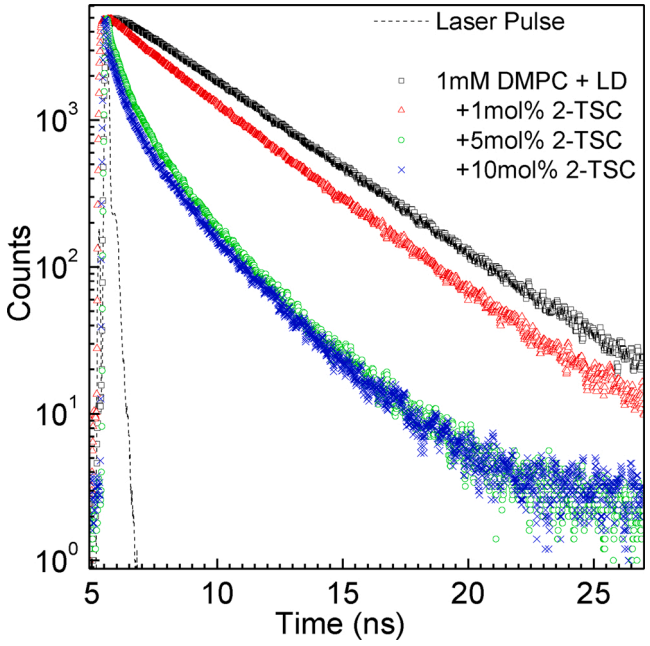

Fig. 8. Decay profiles of the fluorescence intensity of Laurdan in DMPC (1 mM) without and with the addition of different 2-TSC concentrations, at 35 °C. Excitation wavelength at 330 nm, and emission at 480 nm.

3.3. *Fluorescence spectroscopy*

Fig. 6 shows optical absorption and fluorescence emission spectra of the following systems: DMPC/Laurdan, DMPC/2-TSC and DMPC/2-TSC/Laurdan, in the gel phase of the membrane, at 15 °C and in the fluid phase, at 35 °C. The probe Laurdan absorbs in the same wavelength region as that of 2-TSC. Hence, the wavelength used for the Laurdan excitation (330 nm) can also be absorbed by the 2-TSC. However, as shown in Fig. 6, 2-TSC showed no fluorescence when excited at this same wavelength. Thus, Laurdan is a suitable fluorescent probe to monitor the lipid bilayer properties in the presence of 2-TSC. The probe Laurdan, widely used to study phospholipid bilayers (Calori et al., 2019; Leung et al., 2019; Ma et al., 2018), is supposed to be located in the membrane close to the polar head groups of the bilayer (De

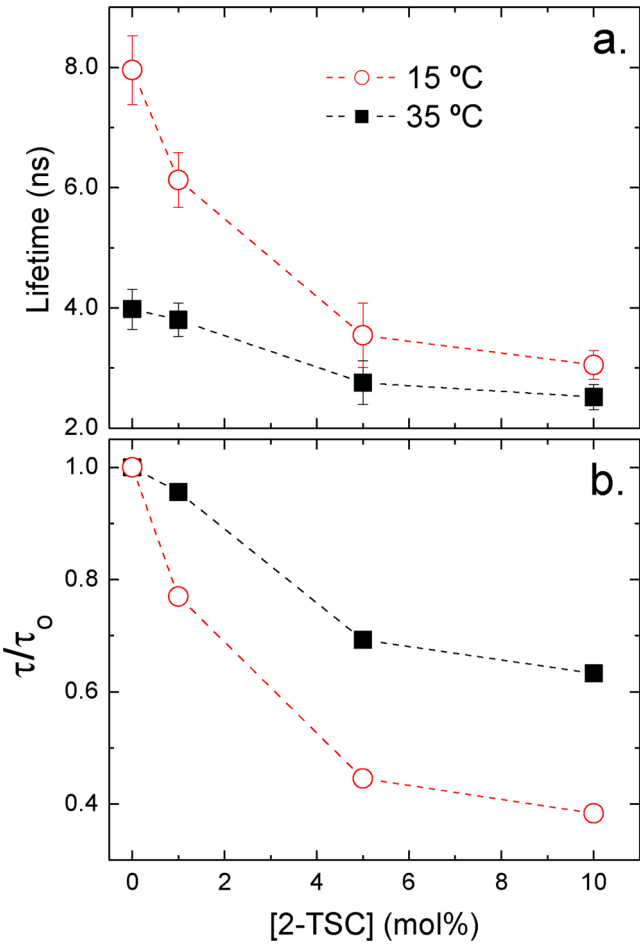

Fig. 9. (a) Values of the longer lifetime found for Laurdan in DMPC as a function of 2-TSC concentration, at 15 and 35°C, using Eq. 2.**(b)** ratios of Laurdan lifetime in the presence (τ) of different 2-TSC concentrations and Laurdan lifetime without 2-TSC (τ_0).

Vequi-Suplicy et al., 2006), and it is very sensitive to changes in the medium polarity as well as changes on the bilayer fluidity.

Still analyzing the spectra of Fig. 6, it is possible to see that 2-TSC seems to act as a quencher of the Laurdan fluorescence, due to the drastic decrease observed in the fluorescence intensity upon addition of 2-TSC to the system.

Experiments were performed at different temperatures in the range between 15 °C and 50 °C. This decrease in the fluorescence intensity of Laurdan was observed in both gel and fluid phases of the DMPC lipid bilayer.

The fluorescence anisotropy of Laurdan is also very sensitive to the presence of the 2-TSC molecule. With 5 mol% of 2-TSC, values of Laurdan anisotropy increase for both DMPC phases, gel and fluid, as can be seen in Fig. 7. Because the 2-TSC quenches the Laurdan fluorescence, it was not possible to obtain plots of the fluorescence anisotropy as a function of the temperature for 10 and 15 mol% of 2-TSC, due to the extremely low fluorescence intensity of Laurdan, which generates large errors in anisotropy values.

When analyzing static fluorescence anisotropy values, it is essential to monitor the variation in the fluorescence lifetime of the probe: if there is a variation in the fluorescence lifetime, care must be taken when interpreting the anisotropy values.

Therefore, we also performed time-resolved fluorescence measurements. Profiles of Laurdan fluorescence intensity decay were measured with excitation at 330 nm and emission at 480 nm and are shown in Fig. 8.

From Fig. 8, it is possible to observe faster decays with the increase of the 2-TSC concentration. The analysis of the lifetimes of Laurdan clearly shows the quenching of its fluorescence by 2-TSC. Since the lifetime decreases, static quenching is discarded, and collisional quenching or Foster Resonance Energy Transfer (FRET) are happening. As usual (Marsh, 2009; Parasassi et al., 1986; Vequi-Suplicy et al., 2013), Laurdan decays could be fitted with two lifetimes, according to Eq. 2, with $\chi^2 \leq 1.1$. Fig. 9 shows the lifetimes (long component lifetime only) of Laurdan in both phases of the lipid bilayer for different values of relative 2-TSC concentration.

The long lifetime component of the fluorescence decay is used here because it was found to predominate at 480 nm, both in gel and fluid DMPC membrane phases. Moreover, in the fluid DMPC phase, it is nearly the only component, around 90 % (Vequi-Suplicy et al., 2013).

Considering that Laurdan is located in the membrane close to the surface, (De Vequi-Suplicy et al., 2006), and that there is a high quenching of its fluorescence by 2-TSC and, which needs a certain proximity between the fluorophore and the quencher during the lifetime of the fluorophore excited state for the quenching mechanism to occur, we can infer that 2-TSC is also closer to the surface, perhaps interspersed in the region of the hydrocarbon chains, just below the polar head groups. This is in accordance with Fig. 3, in which absorption spectra of 2-TSC in ethanol, HEPES Buffer and DMPC suggest that the polarity in the region where the 2-TSC is located must be around 24.5 and 80, that is, in the region close to the polar head groups. The location of molecules in lipid bilayers (Singh et al., 2017, 2016), as well as their distribution in these bilayers (Loura, 2012; Marquezin et al., 2019), is a topic widely studied in the literature, and stating about the location of a molecule in these bilayers is not so simple.

Interestingly, the quenching is more evident in the lipid gel phase (15 °C) than in the fluid phase (35 °C), as can be seem in Fig. 9. Considering a dynamic quenching between 2-TSC and Laurdan, one would expected a more efficient quenching in the fluid than in the gel phase, due to the huge increase in the diffusion coefficient of lipids from gel to fluid membranes, around two orders of magnitude (Korlach et al., 1999), and assuming that the diffusion of a molecule in the bilayer would be modulated by the lipid diffusion. As the opposite is observed, this is an indication that 2-TSC and Laurdan are closer in the gel than in the fluid membrane. At least partially, that could be due to the closer proximity of molecules in a gel bilayer than in a fluid one, as the area per lipid in a gel PC bilayer is supposed to be around 25 % smaller than in the fluid phase (Nagle and Tristram-Nagle, 2000). But could also be related to a change in the location in the bilayer of 2-TSC and/or Laurdan, from one bilayer phase to the other.

On the other hand, considering that there is a small spectral overlap between the Laurdan emission and the absorption of 2-TSC (both in DMPC), FRET occurrence between these two molecules must be considered. In the gel phase all molecules are more rigid, meaning that dipoles would have less rotational freedom, and this could mean that the energy transfer is more likely to happen in the gel phase, if the donor-acceptor dipoles alignment favors it. In the fluid phase, 2-TSC and Laurdan are less hindered and their dipoles can reach a broader range of relative orientations, which could result in less quenching in the membrane fluid phase than in the gel one.

The fact that a decrease in Laurdan lifetime is observed in the presence of 2-TSC means that the static anisotropy values (Fig. 7) should be interpreted more carefully. If the lifetime of an excited state decreases, the fluorescent probe would have less time to depolarize the light during its excitation, thereby increasing the measured anisotropy value. Taking this into account, the values shown in Fig. 7 may be a distortion towards higher values of anisotropy, since the lifetime of the excited state decreases as the 2-TSC concentration increases, as shown in Fig. 9.

3.4. ESR spectroscopy

For a better understanding of the changes caused by 2-TSC on the structure of DMPC membranes, a phosphocholine spin label was incorporated into the membranes.

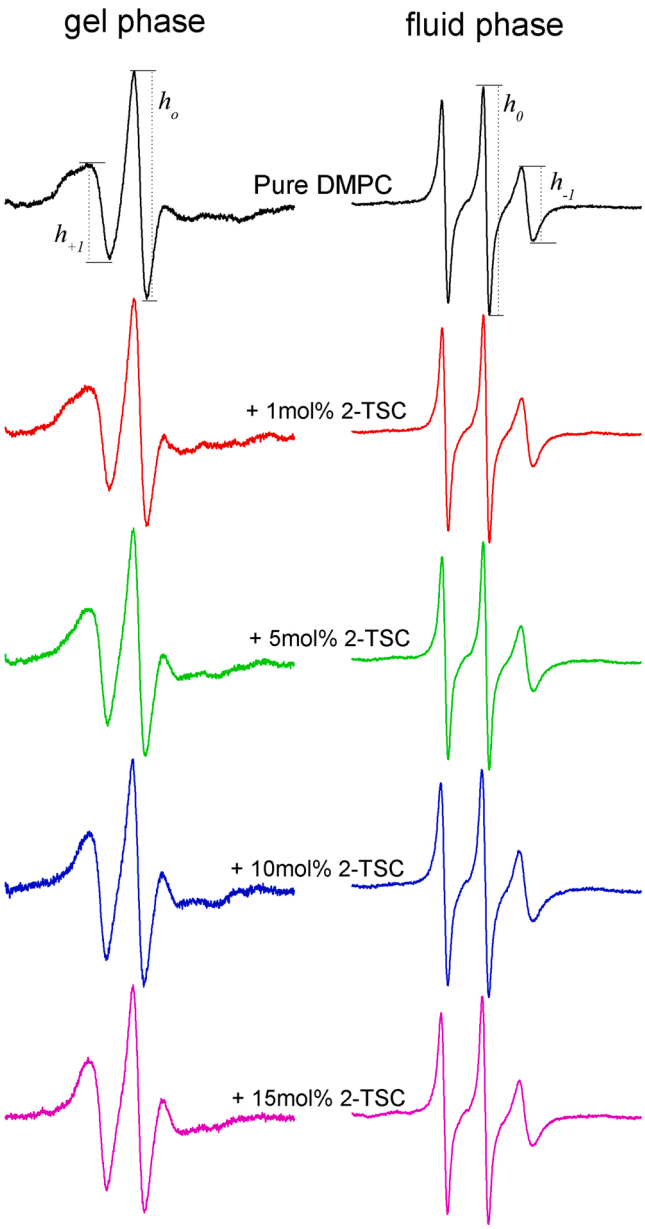

Fig. 10. ESR spectra of 14-PCSL in DMPC vesicles containing different relative concentrations of 2-TSC, as indicated. Spectra were acquired at the gel (10°C) and fluid (40°C) phases of the membrane. The total spectrum width is 100 G. Dotted lines represent the high, central and low field amplitudes.

Structural changes at the DMPC bilayer core, monitored by 14-PCSL (see Fig. 1), caused by the addition of different 2-TSC relative molar concentrations are shown in Fig. 10. The ESR spectra are shown for the DMPC membrane in the gel phase, (10 °C), and in the fluid phase (40 °C), as indicated by DSC analysis (Fig. 2).

The spectra in Fig. 10 are normalized by the maximum signal amplitude. In the gel phase (10 °C), an anisotropic spectrum is observed for pure DMPC vesicles, as expected when a bilayer gel phase is monitored by 14-PCSL (Rozenfeld et al., 2015). In this bilayer phase, the addition of 2-TSC in the DMPC extruded vesicle suspension increases the mobility of the bilayer core monitored by the spin label, as its ESR spectrum becomes typical of a more fluid and/or less organized environment (Rozenfeld et al., 2017). In the fluid phase (40° C), all samples display typical nearly isotropic spectra.

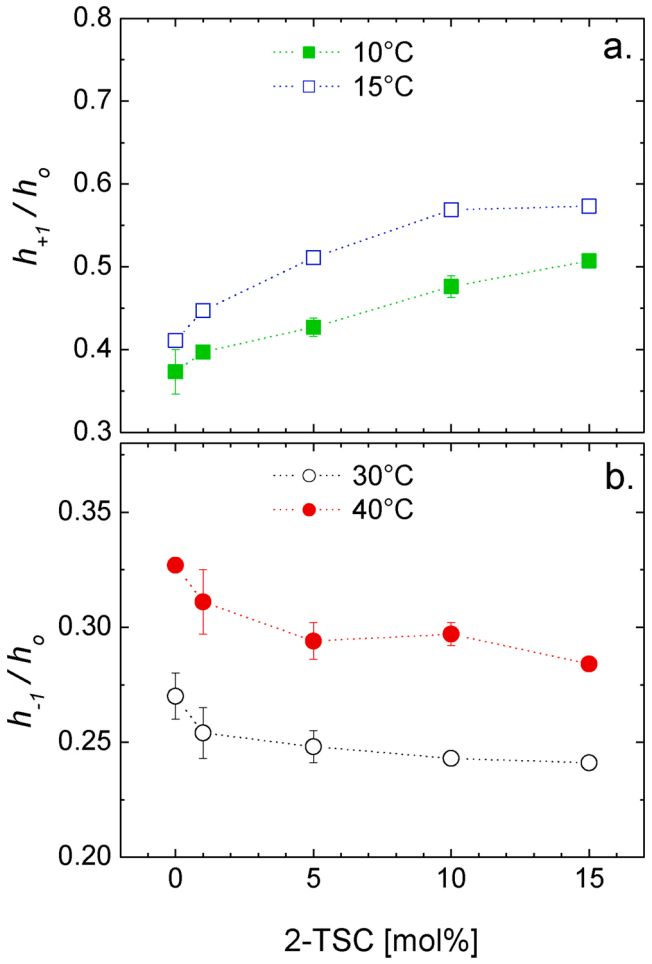

Fig. 11. (a) Ratio between the amplitudes of the low and central field lines (h_{+1}/h_o) of the ESR spectrum of 14-PCSL incorporated in gel phase DMPC bilayers and **(b)** ratio between amplitudes of the high and central field lines (h_{-1}/h_o) of the ESR spectrum of 14-PCSL incorporated DMPC in the fluid phase as a function of 2-TSC molar ratio, relative to the lipid concentration (1 mM). Temperatures are indicated. The plots were obtained from the spectra analysis of Fig. 10.

To better understand the structural alterations caused by 2-TSC on DMPC bilayers, the 14-PCSL ESR spectra were analyzed through the ratio of the amplitudes of the low and central field lines (h_{+1}/h_o) as indicated in Fig. 10, for the spectra yielded by the lipid in the gel phase (at 10 and 15 °C). For the fluid phase (at 30 and 40 °C), the best parameter to be used is the ratio of the amplitudes of the high and central field lines (h_{-1}/h_o): these ratios tend to unity as the spin label mobility increases and/or the probe movement becomes less ordered (Marsh, 1981). As previously described (Rozenfeld et al., 2017), it is useful to measure a h_{+1}/h_o ratio in spectra like that of 14-PCSL in the gel phase, although it is known that it does not correspond to the ratios of the $m_1 = +1$ and *0* hyperfine lines. However, this measurement provides good information on the bilayer structure, as it increases as the bilayer becomes less packed.

In Fig. 11a, h_{+1}/h_o values *versus* 2-TSC concentrations are plotted at 10 °C and 15 °C (gel phase). As expected, the packing of the bilayer decreases with the temperature (h_{+1}/h_o increases). As discussed above, the addition of 2-TSC clearly decreases the packing of DMPC gel phase (increases h_{+1}/h_o).

In the fluid phase, at 30 °C and 40 °C (Fig. 11b), as expected, the packing of the bilayer core also decreases with the temperature (increase in h_{-1}/h_o), but, opposite to what happens in the bilayer gel phase, it increases with the increase of the 2-TSC concentration (decrease in h_{-1}/h_o). Considering this decrease in the fluidity of the bilayer with the increase of 2-TSC concentration, it could be speculated that, in fluid DMPC, 2-TSC is slightly below the lipids polar heads, since it interferes with the mobility/order of the hydrocarbon chains. Though its structure is quite different from cholesterol, it is interesting to note that 2-TSC seems to behave like a cholesterol molecule inserted into lipid bilayers (Bhattacharya and Haldar, 2000; Finean, 1990): it fluidizes the gel phase and rigidifies the fluid phase.

4. Conclusions

From calorimetric measurements it was possible to state that 2-TSC affects the packing of DMPC membranes, strongly decreasing the cooperativity of the gel-fluid bilayer thermal transition. Differences in the optical spectrum of 2-TSC in water medium and in the lipid membrane indicate different structures for the drug in the two environments. Moreover, 2-TSC was found to be more soluble in lipids and ethanol than in water. Despite its aromaticity, 2-TSC displays no fluorescence, but it was found to act as a fluorescence quencher of Laurdan, decreasing Laurdan excited state lifetimes. As Laurdan is known to be localized close to the membrane surface, it can be concluded that this should also be the position of 2-TSC in a lipid membrane. ESR of a spin probe at the membrane core indicates that 2-TSC fluidizes the lipid bilayer gel phase and rigidifies or organizes the bilayer fluid phase. A similar effect is found for other lipophilic molecules, including cholesterol. This work shows that not only 2-TSC has high affinity for lipid membranes, but it also causes changes in the bilayer fluidity. That is certainly relevant for the understanding of the biological activity and cytotoxicity of the drug in organisms.

Declaration of Competing Interest

The authors report no declarations of interest.

Acknowledgments

M.T.L. and C.M.A.O. are recipient of a CNPq research fellowship. M. T.L. and E.L.D. are part of the National Institute of Science and Technology Complex Fluids (INCT-FCx), financed by CNPq (465259/2014-6) and FAPESP (2014/50983-3).

Appendix A. Supplementary data

Supplementary material related to this article can be found, in the online version, at doi:https://doi.org/10.1016/j.chemphyslip.2020.105018.

References

Ali, A.Q., Teoh, S.G., Salhin, A., Eltayeb, N.E., Khadeer Ahamed, M.B., Majid, a.M.S.A., 2014. Synthesis of isatin thiosemicarbazones derivatives: in vitro anti-cancer, DNA binding and cleavage activities. Spectrochim. Acta - Part A Mol. Biomol. Spectrosc. 125, 440–448. https://doi.org/10.1016/j.saa.2014.01.086.

Alonso, L., Marquezin, C.A., Gonçalves, P.J., Alonso, A., 2016. Transmittance and autofluorescence of neonatal rat stratum corneum: nerolidol increases the dynamics and partitioning of protoporphyrin IX into intercellular membranes. J. Fluoresc. 1–9. https://doi.org/10.1007/s10895-015-1758-z.

Alonso, L., Fernandes, K.S., Mendanha, S.A., Gonçalves, P.J., Gomes, R.S., Dorta, M.L., Alonso, A., 2019. In vitro antileishmanial and cytotoxic activities of nerolidol are associated with changes in plasma membrane dynamics. Biochim. Biophys. Acta Biomembr. 1861, 1049–1056.

Asamoto, M., Ota, T., Toriyama-Baba, H., Hokaiwado, N., Naito, A., Tsuda, H., 2002. Mammary carcinomas induced in human c-Ha-ras proto-oncogene transgenic rats are estrogen-independent, but responsive to d-limonene treatment. Jpn. J. Cancer Res. 93, 32–35.

Beebe, S.J., Celestine, M.J., Bullock, J.L., Sandhaus, S., Arca, J.F., Cropek, D.M., Ludvig, T.A., Foster, S.R., Clark, J.S., Beckford, F.A., Tano, C.M., Tonsel-White, E.A., Gurung, R.K., Stankavich, C.E., Tse-Dinh, Y.C., Jarrett, W.L., Holder, A.A., 2020. Synthesis, characterization, DNA binding, topoisomerase inhibition, and apoptosis induction studies of a novel cobalt(III) complex with a thiosemicarbazone ligand. J. Inorg. Biochem. 203, 110907 https://doi.org/10.1016/j.jinorgbio.2019.110907.

Bhattacharya, S., Haldar, S., 2000. Interactions between cholesterol and lipids in bilayer membranes. Role of lipid headgroup and hydrocarbon chain–backbone linkage. Biochim. Biophys. Acta. Biomembr. 1467, 39–53. https://doi.org/10.1016/S0005-2736(00)00196-6.

Britta, E., Scariot, D., Falzirolli, H., Ueda-Nakamura, T., Silva, C., Filho, B., Borsali, R., Nakamura, C., 2014. Cell death and ultrastructural alterations in Leishmania amazonensis caused by new compound 4-Nitrobenzaldehyde thiosemicarbazone derived from S-limonene. BMC Microbiol. 14, 236. https://doi.org/10.1186/s12866-014-0236-0.

Calori, I.R., Pazin, W.M., Brunaldi, K., Pellosi, D.S., Caetano, W., Tedesco, A.C., Hioka, N., 2019. Laurdan as fluorescent probe to determinate the critical micelle temperature of polymers from Pluronic®-coated fluid phase liposomes. J. Mol. Liq. 294, 111562 https://doi.org/10.1016/j.molliq.2019.111562.

Camargos, H.S., Moreira, R.A., Mendanha, S.A., Fernandes, K.S., Dorta, M.L., Alonso, A., 2014. Terpenes increase the lipid dynamics in the Leishmania plasma membrane at concentrations similar to their IC50 values. PLoS One 9. https://doi.org/10.1371/journal.pone.0104429.

Chen, J., Jiang, Q.D., Chai, Y.P., Zhang, H., Peng, P., Yang, X.X., 2016. Natural terpenes as penetration enhancers for transdermal drug delivery. Molecules 21, 1–22. https://doi.org/10.3390/molecules21121709.

Chilom, C.G., Zorilă, B., Bacalum, M., Bălăşoiu, M., Yaroslavtsev, R., Stolyar, S.V., Tyutyunnicov, S., 2020. Ferrihydrite nanoparticles interaction with model lipid membranes. Chem. Phys. Lipids 226, 104851. https://doi.org/10.1016/j.chemphyslip.2019.104851.

da Silva, A.P., Martini, M.V., de Oliveira, C.M.a, Cunha, S., de Carvalho, J.E., Ruiz, A.L.T. G., da Silva, C.C., 2010. Antitumor activity of (-)-alpha-bisabolol-based thiosemicarbazones against human tumor cell lines. Eur. J. Med. Chem. 45, 2987–2993. https://doi.org/10.1016/j.ejmech.2010.03.026.

da Silva, P.R., de Oliveira, J.F., da Silva, A.L., Queiroz, C.M., Feitosa, A.P.S., Duarte, D.M. F.A., da Silva, A.C., de Castro, M.C.A.B., Pereira, V.R.A., da Silva, R.M.F., Alves, L.C., dos Santos, F.A.B., de Lima, Mdo C.A., 2020. Novel indol-3-yl-thiosemicarbazone derivatives: obtaining, evaluation of in vitro leishmanicidal activity and ultrastructural studies. Chem. Biol. Interact. 315, 108899 https://doi.org/10.1016/j.cbi.2019.108899.

Dave, P.C., Inbaraj, J.J., Lorigan, G.A., 2004. Electron paramagnetic resonance studies of magnetically aligned phospholipid bilayers utilizing a phospholipid spin label. Langmuir 20, 5801–5808. https://doi.org/10.1021/la036377a.

de Araújo Neto, L.N., de Lima, Mdo C.A., de Oliveira, J.F., de Souza, E.R., Feitosa Machado, S.E., de Souza Lima, G.M., Silva Buonafina, M.D., Brayner, F.A., Alves, L. C., Sandes, J.M., da Silva, M.V., de Castro, M.C.A.B., Pereira Neves, R., Bezerra Mendonça-Junior, F.J., 2020. Thiophene-thiosemicarbazone derivative (L10) exerts antifungal activity mediated by oxidative stress and apoptosis in C. Albicans. Chem. Biol. Interact. 320. https://doi.org/10.1016/j.cbi.2020.109028.

De Farias Santiago, E., De Oliveira, S.A., De Oliveira Filho, G.B., Magalhaes Moreira, D. R., Teixeira Gomes, P.A., Da Silva, A.L., De Barros, A.F., Da Silva, A.C., Ramos Dos Santos, T.A., Alves Pereira, V.R., Araújo Gonçalves, G.G., Brayner, F.A., Alves, L.C., Wanderley, A.G., Lima Leite, A.C., 2014. Evaluation of the anti-Schistosoma mansoni activity of thiosemicarbazones and thiazoles. Antimicrob. Agents Chemother. 58, 352–363. https://doi.org/10.1128/AAC.01900-13.

De Vequi-Suplicy, C.C., Benatti, C.R., Lamy, M.T., 2006. Laurdan in fluid bilayers: position and structural sensitivity. J. Fluoresc. 16, 431–439. https://doi.org/10.1007/s10895-005-0059-3.

dos Anjos, J.L.V., Alonso, A., 2008. Terpenes increase the partitioning and molecular dynamics of an amphipathic spin label in stratum corneum membranes. Int. J. Pharm. 350, 103–112. https://doi.org/10.1016/j.ijpharm.2007.08.024.

Enoki, T.A., Henriques, V.B., Lamy, M.T., 2012. Light scattering on the structural characterization of DMPG vesicles along the bilayer anomalous phase transition. Chem. Phys. Lipids 165, 826–837. https://doi.org/10.1016/j.chemphyslip.2012.11.002.

Finean, J.B., 1990. Interaction between cholesterol and phospholipid in hydrated bilayers. Chem. Phys. Lipids 54, 147–156. https://doi.org/10.1016/0009-3084(90)90008-F.

Glinma, B., Kpoviessi, S.D.S., Gbaguidi, Fa., Kapanda, C.N., Bero, J., Quetin-Leclercq, J., Moudachirou, M., Poupaert, J., Accrombessi, G.C., Gachomo, E.W., Baba-Moussa, L., Kotchoni, S.O., 2014. Trypanocidal and cytotoxic evaluation of synthesized thiosemicarbazones as potential drug leads against sleeping sickness. Mol. Biol. Rep. 41, 1617–1622. https://doi.org/10.1007/s11033-013-3008-2.

González-Barcia, L.M., Fernández-Fariña, S., Rodríguez-Silva, L., Bermejo, M.R., González-Noya, A.M., Pedrido, R., 2020. Comparative study of the antitumoral activity of phosphine-thiosemicarbazone gold(I) complexes obtained by different methodologies. J. Inorg. Biochem. 203, 110931 https://doi.org/10.1016/j.jinorgbio.2019.110931.

Haag, J.D., Lindstrom, M.J., Gould, M.N., 1992. Limonene induced regression of mammary carcinomas. Cancer Res. 52, 4021–4027.

Haraguchi, S.K., Silva, A.A., Vidotti, G.J., Dos Santos, P.V., Garcia, F.P., Pedroso, R.B., Nakamura, C.V., De Oliveira, C.M.A., Da Silva, C.C., 2011. Antitrypanosomal activity of novel benzaldehyde-thiosemicarbazone derivatives from kaurenoic acid. Molecules 16, 1166–1180. https://doi.org/10.3390/molecules16021166.

Hatta, I., Nakazawa, H., Obata, Y., Ohta, N., Inoue, K., Yagi, N., 2010. Novel method to observe subtle structural modulation of stratum corneum on applying chemical agents. Chem. Phys. Lipids 163, 381–389. https://doi.org/10.1016/j.chemphyslip.2010.02.005.

Heimburg, T., 2007. Thermal biophysics of membranes. Thermal Biophysics of Membranes. Wiley, Weinheim. https://doi.org/10.1002/9783527611591.

Hope, M.J., Bally, M.B., Webb, G., Cullis, P.R., 1985. Production of large unilamellar vesicles by a rapid extrusion procedure. Characterization of size distribution, trapped volume and ability to maintain a membrane potential. BBA - Biomembr. 812, 55–65. https://doi.org/10.1016/0005-2736(85)90521-8.

Jaroque, G.N., Sartorelli, P., Caseli, L., 2020. The effect of the monocyclic monoterpene tertiary alcohol γ-terpineol on biointerfaces containing cholesterol. Chem. Phys. Lipids 230, 104915. https://doi.org/10.1016/j.chemphyslip.2020.104915.

Katsaras, J., Gutberlet, T., 2001. Lipid Bilayers: Structure and Interactions. Springer-Verlag, Berlin, Berlin.

Korlach, J., Schwille, P., Webb, W.W., Feigenson, G.W., 1999. Characterization of lipid bilayer phases by confocal microscopy and fluorescence correlation spectroscopy. Proc. Natl. Acad. Sci. 96, 8461–8466. https://doi.org/10.1073/pnas.96.15.8461.

Lakowicz, J.R. (Ed.), 2006. Principles of Fluorescence Spectroscopy.. Springer US, Boston, MA. https://doi.org/10.1007/978-0-387-46312-4.

Lawrence, M.L., Shell, S.M., Beckford, F.A., 2020. Binuclear manganese-iron complexes containing ferrocenyl thiosemicarbazones: Biological activity and carbon monoxide-releasing properties. Inorganica Chim. Acta 507, 119548. https://doi.org/10.1016/j.ica.2020.119548.

Leung, S.S.W., Brewer, J., Bagatolli, L.A., Thewalt, J.L., 2019. Measuring molecular order for lipid membrane phase studies: linear relationship between Laurdan generalized polarization and deuterium NMR order parameter. Biochim. Biophys. Acta Biomembr. 1861, 183053 https://doi.org/10.1016/j.bbamem.2019.183053.

Lim, P.F.C., Liu, X.Y., Kang, L., Ho, P.C.L., Chan, Y.W., Chan, S.Y., 2006. Limonene GP1/PG organogel as a vehicle in transdermal delivery of haloperidol. Int. J. Pharm. 311, 157–164. https://doi.org/10.1016/j.ijpharm.2005.12.042.

Loura, L., 2012. Lateral distribution of NBD-PC fluorescent lipid analogs in membranes probed by molecular dynamics-assisted analysis of förster resonance energy transfer (FRET) and fluorescence quenching. Int. J. Mol. Sci. 13, 14545–14564. https://doi.org/10.3390/ijms131114545.

Ma, Y., Benda, A., Kwiatek, J., Owen, D.M., Gaus, K., 2018. Time-resolved laurdan fluorescence reveals insights into membrane viscosity and hydration levels. Biophys. J. 115, 1498–1508. https://doi.org/10.1016/j.bpj.2018.08.041.

Magalhaes Moreira, D.R., De Oliveira, A.D.T., Teixeira De Moraes Gomes, P.A., De Simone, C.A., Villela, F.S., Ferreira, R.S., Da Silva, A.C., Dos Santos, T.A.R., Brelaz De Castro, M.C.A., Pereira, V.R.A., Leite, A.C.L., 2014. Conformational restriction of aryl thiosemicarbazones produces potent and selective anti-Trypanosoma cruzi compounds which induce apoptotic parasite death. Eur. J. Med. Chem. 75, 467–478. https://doi.org/10.1016/j.ejmech.2014.02.001.

Maqbool, S.N., Lim, S.C., Park, K.C., Hanif, R., Richardson, D.R., Jansson, P.J., Kovacevic, Z., 2020. Overcoming tamoxifen resistance in oestrogen receptor-positive breast cancer using the novel thiosemicarbazone anti-cancer agent. DpC. Br. J. Pharmacol 1–16. https://doi.org/10.1111/bph.14985.

Marquezin, C.A., Ito, A.S., de Souza, E.S., 2019. Organization and dynamics of NBD-labeled lipids in lipid bilayer analyzed by FRET using the small membrane fluorescent probe AHBA as donor. Biochim. Biophys. Acta Biomembr. 1861, 182995 https://doi.org/10.1016/j.bbamem.2019.05.017.

Marsh, D., 1981. Electron spin resonance: spin labels. In: Grell, E. (Ed.), Molecular Biology Biochemistry and Biophysics: Membrane Spectroscopy. Springer, Berlin Heidelberg, New York, pp. 51–142.

Marsh, D., 1990. Handbook of Lipids Bilayers. CRC, Boca Raton.

Marsh, D., 2009. Reaction fields in the environment of fluorescent probes: polarity profiles in membranes. Biophys. J. 96, 2549–2558. https://doi.org/10.1016/j.bpj.2009.01.006.

Mendanha, S.A., Alonso, A., 2015. Effects of terpenes on fluidity and lipid extraction in phospholipid membranes. Biophys. Chem. 198, 45–54. https://doi.org/10.1016/j.bpc.2015.02.001.

Mendanha, S.A., Marquezin, C.A., Ito, A.S., Alonso, A., 2017. Effects of nerolidol and limonene on stratum corneum membranes: a probe EPR and fluorescence spectroscopy study. Int. J. Pharm. 532, 547–554. https://doi.org/10.1016/j.ijpharm.2017.09.046.

Menezes, L.R.A., Santos, N.N., Meira, C.S., Ferreira Dos Santos, J.A., Guimarães, E.T., Soares, M.B.P., Nepel, A., Barison, A., Costa, E.V., 2014. A new source of (R)-limonene and rotundifolone from leaves of Lippia pedunculosa (Verbenaceae) and their trypanocidal properties. Nat. Prod. Commun. 9, 737–739.

Mohamed, Na., Mohamed, R.R., Seoudi, R.S., 2014. Synthesis and characterization of some novel antimicrobial thiosemicarbazone O-carboxymethyl chitosan derivatives. Int. J. Biol. Macromol. 63, 163–169. https://doi.org/10.1016/j.ijbiomac.2013.10.044.

Mourey, a., Canillac, N., 2002. Anti-Listeria monocytogenes activity of essential oils components of conifers. Food Control 13, 289–292. https://doi.org/10.1016/S0956-7135(02)00026-9.

Nagle, J.F., Tristram-Nagle, S., 2000. Structure of lipid bilayers. Biochim. Biophys. Acta - Rev. Biomembr. https://doi.org/10.1016/S0304-4157(00)00016-2.

Osella, S., Smisdom, N., Ameloot, M., Knippenberg, S., 2019. Conformational changes as driving force for phase recognition: the case of Laurdan. Langmuir 35, 11471–11481. https://doi.org/10.1021/acs.langmuir.9b01840.

Ozturk, S., Ercisli, S., 2006. The chemical composition of essential oil and in vitro antibacterial activities of essential oil and methanol extract of Ziziphora persica Bunge. J. Ethnopharmacol. 106, 372–376. https://doi.org/10.1016/j.jep.2006.01.014.

Parasassi, T., Conti, F., Gratton, E., 1986. Time-resolved fluorescence emission spectra of Laurdan in phospholipid vesicles by multifrequency phase and modulation fluorometry. Cell. Mol. Biol. 32, 103–108.

Pérez, H.A., Disalvo, A., de Los Angeles Frias, M., 2019. Effect of cholesterol on the surface polarity and hydration of lipid interphases as measured by Laurdan fluorescence: new insights. Colloids Surf. B Biointerfaces 178, 346–351. https://doi.org/10.1016/j.colsurfb.2019.03.022.

Riske, K.A., Barroso, R.P., Vequi-Suplicy, C.C., Germano, R., Henriques, V.B., Lamy, M.T., 2009. Lipid bilayer pre-transition as the beginning of the melting process. Biochim. Biophys. Acta Biomembr. 1788, 954–963. https://doi.org/10.1016/j.bbamem.2009.01.007.

Rozenfeld, J.H.K., Duarte, E.L., Ruysschaert, J.-M., Lonez, C., Lamy, M.T., 2015. Structural characterization of novel cationic diC16-amidine bilayers: evidence for partial interdigitation. Biochim. Biophys. Acta Biomembr. 1848, 127–133. https://doi.org/10.1016/j.bbamem.2014.10.013.

Rozenfeld, J.H.K., Duarte, E.L., Oliveira, T.R., Lamy, M.T., 2017. Structural insights on biologically relevant cationic membranes by ESR spectroscopy. Biophys. Rev. 9, 633–647. https://doi.org/10.1007/s12551-017-0304-4.

Shyamsivappan, S., Vivek, R., Saravanan, A., Arasakumar, T., Suresh, T., Athimoolam, S., Mohan, P.S., 2020. A novel 8-nitro quinoline-thiosemicarbazone analogues induces G1/S & G2/M phase cell cycle arrest and apoptosis through ROS mediated mitochondrial pathway. Bioorg. Chem. 97, 103709 https://doi.org/10.1016/j.bioorg.2020.103709.

Singh, P., Shukla, R., Prakash, B., Kumar, A., Singh, S., Mishra, P.K., Dubey, N.K., 2010. Chemical profile, antifungal, antiaflatoxigenic and antioxidant activity of Citrus maxima Burm. And Citrus sinensis (L.) Osbeck essential oils and their cyclic monoterpene, DL-limonene. Food Chem. Toxicol. 48, 1734–1740. https://doi.org/10.1016/j.fct.2010.04.001.

Singh, M.K., Shweta, H., Khan, M.F., Sen, S., 2016. New insight into probe-location dependent polarity and hydration at lipid/water interfaces: comparison between gel- and fluid-phases of lipid bilayers. Phys. Chem. Chem. Phys. 18, 24185–24197. https://doi.org/10.1039/C6CP01201A.

Singh, M.K., Khan, M.F., Shweta, H., Sen, S., 2017. Probe-location dependent resonance energy transfer at lipid/water interfaces: comparison between the gel- and fluid-phase of lipid bilayer. Phys. Chem. Chem. Phys. 19, 25870–25885. https://doi.org/10.1039/C7CP03108D.

Soares, R.O.a, Echevarria, A., Bellieny, M.S.S., Pinho, R.T., de Leo, R.M.M., Seguins, W. S., Machado, G.M., Canto-Cavalheiro, M.M., Leon, L.L., 2011. Evaluation of thiosemicarbazones and semicarbazones as potential agents anti-Trypanosoma cruzi. Exp. Parasitol. 129, 381–387. https://doi.org/10.1016/j.exppara.2011.08.019.

Trotsko, N., Golus, J., Kazimierczak, P., Paneth, A., Przekora, A., Ginalska, G., Wujec, M., 2020. Design, synthesis and antimycobacterial activity of thiazolidine-2,4-dione-based thiosemicarbazone derivatives. Bioorg. Chem. 97, 103676 https://doi.org/10.1016/j.bioorg.2020.103676.

Valeur, B., 2001. Molecular fluorescence. Molecular Fluorescence. https://doi.org/10.1002/3527600248.

Vandresen, F., Falzirolli, H., Almeida Batista, Sa., Da Silva-Giardini, A.P.B., De Oliveira, D.N., Catharino, R.R., Ruiz, A.L.T.G., De Carvalho, J.E., Foglio, M.A., Da Silva, C.C., 2014. Novel R-(+)-limonene-based thiosemicarbazones and their antitumor activity against human tumor cell lines. Eur. J. Med. Chem. 79, 110–116. https://doi.org/10.1016/j.ejmech.2014.03.086.

Vequi-Suplicy, C.C., Lamy, M.T., Marquezin, Ca., 2013. The new fluorescent membrane probe Ahba: a comparative study with the largely used Laurdan. J. Fluoresc. 23, 479–486. https://doi.org/10.1007/s10895-013-1172-3.

Yamaguchi, M.U., Da Silva, A.P.B., Ueda-Nakamura, T., Filho, B.P.D., Da Silva, C.C., Nakamura, C.V., 2009. Effects of a thiosemicarbazide camphene derivative on Trichophyton mentagrophytes. Molecules 14, 1796–1807. https://doi.org/10.3390/molecules14051796.

Yildirim, H., Guler, E., Yavuz, M., Ozturk, N., Kose Yaman, P., Subasi, E., Sahin, E., Timur, S., 2014. Ruthenium (II) complexes of thiosemicarbazone: synthesis, biosensor applications and evaluation as antimicrobial agents. Mater. Sci. Eng. C 44, 1–8. https://doi.org/10.1016/j.msec.2014.08.007.

Yu, Y., Kalinowski, D.S., Kovacevic, Z., Siafakas, A.R., Jansson, P.J., Stefani, C., Lovejoy, D.B., Sharpe, P.C., Bernhardt, P.V., Richardson, D.R., 2009. Thiosemicarbazones from the old to new: Iron chelators that are more than just ribonucleotide reductase inhibitors. J. Med. Chem. 52, 5271–5294. https://doi.org/10.1021/jm900552r.